

# Accepted manuscript doi: 10.1680/jgein.19.00036

---

## **Accepted manuscript**

As a service to our authors and readers, we are putting peer-reviewed accepted manuscripts (AM) online, in the Ahead of Print section of each journal web page, shortly after acceptance.

## **Disclaimer**

The AM is yet to be copyedited and formatted in journal house style but can still be read and referenced by quoting its unique reference number, the digital object identifier (DOI). Once the AM has been typeset, an 'uncorrected proof' PDF will replace the 'accepted manuscript' PDF. These formatted articles may still be corrected by the authors. During the Production process, errors may be discovered which could affect the content, and all legal disclaimers that apply to the journal relate to these versions also.

## **Version of record**

The final edited article will be published in PDF and HTML and will contain all author corrections and is considered the version of record. Authors wishing to reference an article published Ahead of Print should quote its DOI. When an issue becomes available, queuing Ahead of Print articles will move to that issue's Table of Contents. When the article is published in a journal issue, the full reference should be cited in addition to the DOI.

# Accepted manuscript doi: 10.1680/jgein.19.00036

---

**Submitted:** 14 December 2018

**Published online in ‘accepted manuscript’ format:** 05 June 2019

**Manuscript title:** Field load tests and modelling of soft foundation reinforced by soilbags

**Authors:** Liujiang Wang<sup>1</sup>, Sihong Liu<sup>1</sup>, Jie Liao<sup>1</sup> and Kewei Fan<sup>1</sup>

**Affiliation:** <sup>1</sup>College of Water Conservancy and Hydropower, Hohai University, Nanjing, 210098, China

**Corresponding author:** Sihong Liu, College of Water Conservancy and Hydropower, Hohai University, Nanjing, 210098, China.

**E-mail:** [sihongliu@hhu.edu.cn](mailto:sihongliu@hhu.edu.cn)

## **Abstract**

A study was performed to investigate the bearing capacity of foundations reinforced by soilbags filled with excavated soft soils by conducting field load tests and numerical analysis. The effect of the number of reinforcement layers on bearing capacity of the soilbag-reinforced foundation was investigated. Both the experimental and numerical studies indicated that soilbag reinforcement with reused excavated soft soils as the contained soilbag material can substantially improve the bearing capacity of the soft foundation and reduce settlement under vertical loading conditions. The bearing capacity was also found to increase with increasing number of soilbag reinforcement layers. The numerical analysis indicated that stress dispersion occurred through the soilbag reinforcement to reduce the load transferred to the underlying soft soils. High-quality compaction of the soilbag layers during construction is very important to improve bearing capacity. In addition, the excess pore water pressure generated in the soft foundation was less with the soilbag reinforcement and decreased with increasing number of reinforcement layers due to the relatively high permeability of the soilbag reinforcement.

**Keywords:** Geosynthetics, Soilbag-reinforced soft foundation, Bearing capacity, Field load test

## Introduction

Soilbags are expandable three-dimensional (3D) geosynthetic containers made from bags made of high-density polythene (PE) or polypropylene (PP). They were originally used to prevent soil flow due to floodwater and to build temporary structures in case of emergency (Kim et al. 2004). Studies by Matsuoka et al. (1999, 2000a, 2003, 2006) revealed the many advantages of soilbags, such as their environmental friendliness, and ability to improve the bearing capacity of soft ground, reduce traffic-induced vibration, and prevent frost heave. It was also found that bags made of polythene (PE) or polypropylene (PP) are stable in both acidic and alkali environments. Furthermore, bags protected from exposure to sunlight (via burial) are very durable. Because of these attributes, the use of soilbags has been extended to permanent or semi-permanent projects, such as soft soil foundation reinforcement (Matsuoka and Liu 2006; Liu and Matsuoka 2007; Xu et al. 2008; Li et al. 2013), expansive soil treatment (Liu et al. 2012, 2015; Wang et al. 2015), base vibration isolation (Liu et al. 2014), retaining wall construction (Lee et al. 2013; Wen et al. 2016; Miyata et al. 2015), coastal protection projects (Martinelli et al. 2011; Hornsey et al. 2011; Kim et al. 2015; Moreira et al. 2016), and soil railway embankment reinforcement (Matsuoka and Liu. 2006; Indraratna et al. 2014).

Bearing capacity and soft soil foundation settlement are great concerns for engineers and researchers working on geotechnical and civil engineering projects. Over the last few decades, due to increasing infrastructural development demands and land use restrictions, geosynthetic reinforcement has been accepted as an effective way to allow structural construction on soft foundation soils (Basudhar et al. 2008; Bergado and Teerawattanasuk. 2008; Rowe and Taechakumthorn. 2008, 2011; Indraratna et al. 2010). Recently, soilbags were found to improve the bearing capacity of soft foundations because when a soilbag is exposed to external forces or building loads, tensile forces occurs along the bag, which in turn provide significant lateral confinement to the wrapped soils and enhance the bearing capability of the soilbag. Matsuoka and Liu (2003) found that soilbags have a high compressive strength (up to nearly 3 MPa approximately one-tenth that of typical concrete) and increase the bearing capacity of soft ground 5-10 times. Shao et al. (2005) and Xu et al. (2007) used soilbags to fill ponds for highway embankment construction and found that they could effectively reduce the settlement of subgrade and significantly decrease costs. Xu et al. (2008) investigated the strength properties of soilbags using unconfined compression tests and bearing capacity tests on real soilbags. However, in the above studies, the infilled materials of soilbags are mainly coarse granular materials or low-cohesion soils like sands and gravels, which are always lacked at the construction site and have to be taken from other places. This will significantly increase the engineering cost and induce some expropriation and environmental problems. Recently, Liu et al. (2019) used soilbags filled with excavated clayey soils to construct retaining wall and found they have high compressive strengths resulting from the tensile forces of woven bags. This indicated that soilbags filled with soft soils could also be used to improve the soft foundation. Recently, the bearing capacity improvement by using soilbags was investigated using small scale tests and 3D numerical

modelling (Hataf and Sayadi. 2018). Nevertheless, the bearing capacity of soilbag-reinforced foundation using excavated soft soil has rarely studied according to the field load test.

In this paper, a series of field load tests are conducted to investigate the bearing capacity of soft foundations reinforced by soilbags filled with excavated soft soils. The bearing capacities of soft foundations with and without soilbag reinforcement are compared to illustrate the effectiveness of the soilbag-reinforced foundation with excavated soft soils reused. In addition, the effect of the number of layers of the soilbag reinforcement on bearing capacity are investigated. Along with numerical analysis, the development and distribution of the vertical earth pressure and pore water pressure during the loading process are also studied and compared with the experimental results.

### **1. Brief introduction to the field bearing capacity tests**

The test site was located at the Xiaoqing River, north of Jinan in the Shandong Province, China, where a large conveyance culvert was to be constructed. This soft foundation was planned to be reinforced using cement mixing piles for the construction of the conveyance culvert initially. However, due to the tight construction schedule and the high cost of cement mixing piles, an alternative ground improvement method using soilbags with excavated soft soils infilled was proposed. Thus, a field load test was conducted to estimate the performance of the foundation reinforced by soilbags filled with excavated soft soils, and the results were compared with those achieved with an unreinforced foundation. Because of the conveyance culvert was buried under ground, the ground was excavated to the designing level during construction. The excavation depth was approximately 4-5 m from the original ground surface, the excavated soil was mainly made up of sandy clay. Therefore, the load tests were performed on an excavated soft foundation pit, the area of the test field is  $60 \times 20$  m, the soils under the loading plate is soft silty clay with the thickness up to 10 m. The groundwater table was roughly 0.4-0.7 m below the excavated surface. The geotechnical properties of the silty clay, given in Table 1, were provided by the Shandong Survey and Design Institute of Water Conservancy based on laboratory tests on soil samples from the field.

Tests were performed on an unreinforced soft foundation, a foundation reinforced by two layers of soilbag reinforcement ( $n = 2$ ) and a foundation reinforced by four layers of soilbag reinforcement ( $n = 4$ ). It is worth noting that the excavated sandy clay was reused as infilled materials of the soilbag in this project to save the cost and shorten the construction period. The bags used to contain sandy clays were made of a black woven polypropylene (PE) geotextile. The properties of the PE bags are as follows: the mass per square metre is 100 g, the warp and weft tensile strengths are 23.4 and 18.8 kN/m, respectively, the warp and weft elongations are both less than 18%, and the warp and weft tensile modulus are 134 and 112 kN/m, respectively. Approximately 45-50 kg of the excavated sandy clay with water content ( $18\% \pm 3\%$ ) was used to fill each bag, and the mouths of the bags were sealed with a manual sewing machine. After that, a shallow foundation pit with an area of  $3 \text{ m} \times 3 \text{ m}$  was excavated at the test position. Then, the soilbags were placed and compacted layer by layer using a plate vibrator. The soilbags had to be staggered to ensure structural integrity. After compaction, each soilbag has approximate dimensions of  $50 \text{ cm} \times 50 \text{ cm} \times 10 \text{ cm}$  (length  $\times$

width  $\times$  height). After compaction, the sandy clay contained in the soilbags was sampled and tested according to the corresponding laboratory tests. The geotechnical properties of the sandy clay are also listed in Table 1. Due to the dynamic compaction, the pre-consolidation stress for the sandy clay in the soilbag is about 80kPa.

The procedure of the field load tests is shown in Fig. 1. A square steel plate with a thickness of 30 mm and 1-m sides was used as the load plate. Fig. 1(a) shows the load test on the unreinforced soil foundation, and the load test on the foundation reinforced by soil bags is shown in Fig. 1(b). In order to reduce experimental error, three parallel tests were conducted for each case. The load was applied in stages. At each stage, the load was held constant until the resulting foundation settlement rate decreased to 0.5 mm/h (after which the next load increment was applied). In this test, the earth pressure and pore water pressure were also measured, the layout of transducers was shown in Fig. 2. To install the transducers in the natural soil, the soil was excavated and then backfilled after the transducers were placed, as illustrated in Fig. 3. However, the earth pressure and pore water pressure were only measured once for each case. The ultimate bearing capacity is determined according to the failure in the ground, and the results of the plate load tests are listed in Table 2. The ultimate bearing capacities of the three cases are 96, 135 and 170 kPa, respectively. The bearing capacity of the reinforced foundation is larger than that of the unreinforced foundation, and it increases with increased layers of soilbag reinforcement. Besides, an increase in the elastic modulus of the soilbag-reinforced foundation was given by back calculation using Boussinesq's solution and loading-settlement curve test results. It can be found that soilbags infilled with excavated soft soils used to reinforce the soft foundations can increase bearing capacity and reduce footing settlement.

## **2. Numerical modelling**

### *2.1 Simulation method*

The objective of the numerical simulation was to reproduce the field load tests described in the previous section and further investigate the reinforcement mechanism of the soilbags filled with excavated soft soils. The simulation was conducted using a finite element method (FEM). So far, a few studies on the numerical modelling of soilbags have been conducted with the soil and bags modelled separately by FEM. (Muramatsu et al. 2007, 2009; Tantonio and Bauer 2008; Ansari et al. 2011; Ye et al. 2011). In these studies, truss elements were used to model the tensile behaviour of PE or PP bags. Muramatsu et al. (2007, 2009) and Ye et al. (2011) analysed the settlement of soilbag foundations under vertical load and vibration damping effect of soilbags, respectively. Tantonio and Bauer (2008) discussed the effect of the soil-geotextile interface (slip/rotation) on stress and strain for soils wrapped in a soilbag. Ansari et al. (2011) developed a 3D FE model, which allows for the consideration of large interfacial slips, surface separation and closure, and numerically analysed the mechanical behaviour of a soilbag subject to compression and lateral cyclic shear loading. However, due to the complexity interfacial relationship between contained soils and geotextile bag, geotextile bag and geotextile bag for above soilbag modelling methods, a limited analysis

was performed on the structures reinforced by soilbags in a real project. Hence, equivalent composite approach (ECA), which has been widely used in many previous studies to model geocell-reinforced structures in different projects (Bathurst and Knight. 1998; Chen et al. 2013a, b; Hegde and Sitharam 2013; Leshchinsky and Ling 2013; Mehdipour et al. 2013; Rahimi et al. 2018a, b; Song et al. 2017, 2018), was used in this study to model the soilbag-reinforced foundation for its simplicity and high computational efficiency.

In the ECA method, the soilbag-reinforced soil was treated as a composite material with the improved strength and stiffness parameters, and its constitutive model is similar to the unreinforced soils. For the geocell-reinforced soil, the triaxial compression test results by Bathurst and Karpurapu (1993), Rajagopal et al. (1999) and Chen et al. (2013b) indicated that an apparent cohesion was induced in the reinforced granular soil due to geocell confinement, but the friction angle of the reinforced soil was basically the same as that of the unreinforced soil. This phenomenon was also found by the laboratory biaxial compression tests on model soilbags and their DEM simulation under compression without consider the particle crushing of the material warped inside the bags (Matsuoka et al. 2003, 2006; Cheng et al. 2016a, b; Liu et al. 2018). Considering the infilled material of soilbag was soft soils and a low vertical stress was applied in the load test, so the friction angle of the soilbag-reinforced soil was assumed to be the same as that of contained in the bag; only apparent cohesion  $c_T$  was considered for the soil reinforced by soilbags.

Fig. 4(a) shows a soilbag subjected to external principal stresses  $\sigma_1$  and  $\sigma_3$  in a two-dimensional manner (Matsuoka et al. 2000b, 2003, 2006; Xu et al. 2008; Liu et al. 2018). Under the actions of  $\sigma_1$  and  $\sigma_3$ , the soilbag usually tends to be flat, accompanied by the extension of the total perimeter of the bag. As a result, a tensile force  $T$  is produced along the bag, which in turn produces an additional stress on the soil particles inside the bag. The components of the additional stress are expressed as:

$$\sigma_{01} = \frac{2T}{B}; \quad \sigma_{03} = \frac{2T}{H} \quad (1)$$

where  $B$  and  $H$  are the width and height of the soilbag, respectively. Thus, the stresses acting on the soil wrapped in the bag are the combined result of the externally applied stresses and the apparently produced stresses by the bag tensile force  $T$ , as shown in Fig. 4(b). At failure, the following equation holds:

$$\sigma_1 + \frac{2T}{B} = K_p \left( \sigma_3 + \frac{2T}{H} \right) \quad (2)$$

where  $K_p = (1 + \sin\varphi)/(1 - \sin\varphi)$  and  $\varphi$  is the internal friction angle of the wrapped soil. As the width  $B$  is usually greater than the height  $H$  for soilbag, it is known from Eq. (1) that the tensile force  $T$  induced along the bag causes stronger confinement to the wrapped soil in the  $\sigma_3$  direction than in the  $\sigma_1$  direction. Thus, the larger the ratio of  $B/H$  of the soilbag is, the more the reinforcement effect is.

By comparing Eq. (2) with the strength expression of  $\sigma_1 = \sigma_3 K_p + 2c\sqrt{K_p}$  for a cohesive-frictional material, the following expression of the apparent cohesion of the soilbag resulting from the bag tension  $T$  is obtained.

$$c_T = \frac{T}{B\sqrt{K_p}} \left( \frac{B}{H} K_p - 1 \right) \quad (3)$$

Considering there is no relative shear deformation between the soilbags when they are used to reinforce the foundations. Thus, the soilbag reinforcement can be treated as a cohesive-frictional material with an apparent cohesion  $c_T$  as expressed in Eq. (3) and a same internal friction angle  $\varphi$  as that of the soils contained in the bags. That is to say, the high compressive strength of the soilbags can be interpreted as the contribution of an apparent cohesion  $c$  resulting from the tension of the bag. For cohesive-frictional materials, a bonding stress  $\sigma_0 (= c_T \cdot \cot\varphi)$  was introduced to reflect the effect of cohesion to their stress-strain relationship by Matsuoka and Sun. (1995). Then, it was successfully applied to reflect the increase of cohesion of unsaturated soil with suction  $s$  and establish an elastoplastic model by Matsuoka et al. (2002). Based on this method, the translated stress  $\hat{\sigma}$  tensor used in the constitutive model for soilbag-reinforced soil is defined as follows:

$$\hat{\sigma}_{ij} = \sigma_{ij} + \sigma_0 \delta_{ij} \quad (4)$$

where  $\sigma_{ij}$  is the stress tensor,  $\delta_{ij}$  is Kronecker's delta.

The axial strain in the height direction of the soilbags is given by  $\varepsilon_a = (H_0 - H)/H_0$ , the volume of soilbags is assumed to be invariable and constant (Matsuoka and Liu 2006), i.e.  $B_0 H_0 = BH$ , and  $B = B_0/(1 - \varepsilon_a)$  is obtained, where  $H_0$  and  $B_0$  are the initial height and width of the soilbags, respectively. In this case, the circumferential extension strain of the woven bags can be obtained as:

$$\varepsilon_c = \frac{\varepsilon_a + m - 1}{(m + 1)(1 - \varepsilon_a)} \varepsilon_a \quad (5)$$

where  $m = B_0/H_0$  is the ratio of the initial width of the soilbags to its height. The tensile force of the bags is written as  $T = k\varepsilon_c$ , where  $k$  is the tensile modulus of PP or PE bags, which can be determined by the ratio of the tensile strength to the maximum extension strain of the bags. Thus, the apparent cohesion of soilbags in Eq (3) can be rewritten as:

$$c_T = \frac{k\varepsilon_a \sqrt{K_p}}{B_0} \frac{\varepsilon_a + m - 1}{(m + 1)(1 - \varepsilon_a)} \left[ \frac{m}{1 - \varepsilon_a} - \frac{1 - \varepsilon_a}{\sqrt{K_p}} \right] \quad (6)$$

It is worth noting that axial strain and apparent cohesion in Eq. (6) for each soilbag should be updated with the settlement of foundation after each time step in the numerical simulation of the field load test. The distribution and evolution of the apparent cohesion in soilbag layers under compression condition is discussed in section 3.4.

## 2.2 Mesh and constitutive model

Numerical predictions were made using the plane strain FE method with ECA to model the soilbag reinforcement. The FE mesh and the boundary conditions are illustrated in Fig. 5. Due to symmetry, only half the foundation was modelled; the modelled area had a horizontal width of 10.0 m and a vertical thickness of 6.0 m. At the left and right boundaries, horizontal displacement was fixed, but vertical displacement was variable. At the bottom boundary, both the horizontal and vertical displacements were fixed. The ground surface (drainage boundary) was considered completely permeable, and the left, right and bottom boundaries were considered impermeable.

In the present study, the modified Cam-clay (MCC) model, which is a widely accepted elastoplastic model for describing the stress-strain behaviour of saturated clay, was adopted. To represent the confinement of the bags to the infilled soil, the original stress variable in the MCC model was replaced by the translated stress defined in Eq. (5). Thus, according to the associated flow rule, the yield and plastic potential functions can be expressed as:

$$f = g = q^2 - M^2 \hat{p}' (\hat{p}_c - \hat{p}') \quad (7)$$

where  $\hat{p}'$  and  $q$  are the translated mean effective stress and deviatoric stress, respectively,  $M$  is the slope of the critical state line (CSL) in the  $q - \hat{p}'$  plane, and  $\hat{p}_c$  is the pre-consolidation pressure, which is the hardening parameter of the model and can be expressed by:

$$\hat{p}_c = \hat{p}_{c0} \exp \left[ \frac{(1 + e_0) \Delta \varepsilon_v^p}{\lambda - \kappa} \right] \quad (8)$$

where  $\lambda$  and  $\kappa$  are the plastic compression index and unloading-reloading index, respectively,  $e_0$  is the initial void ratio,  $\Delta \varepsilon_v^p$  is the increment of plastic volumetric strain, and  $\hat{p}_{c0}$  is the translated pre-consolidation pressure at the beginning of plastic loading.

The numerical analyses were performed using the fully hydro-mechanical coupling FE code developed by the Institute of Hydraulic Structures of Hohai University (Wang et al. 2015; Liu et al. 2016).

## 2.3 Determination of model parameters

Table 3 shows the model parameters used in the numerical simulations, as estimated from the experimental results given in Table 1. Plastic compression index  $\lambda$  was back-calculated from given compression index  $C_c$  using the relationship  $\lambda = C_c/2.3$ . Ratio  $\lambda/\kappa$  generally varies in the range 5–10; 10 was chosen in these analyses so that  $\kappa = 0.1\lambda$ . For triaxial compression conditions, the slope of the critical state line in the  $p'-q$  plane,  $M = 6\sin\phi/(3 - \sin\phi)$ , was calculated. Poisson's ratio was assumed to be 0.3. In the elastic region of soil behaviour, Young's modulus was adopted as the usual function of mean effective stress and initial void ratio. Because the load test was conducted on the excavated foundation

pit with soils in the unloading state, a value of Young's modulus corresponding to  $p' = 100$  kPa was assumed in these analyses when the initial effective mean stress was less than 100 kPa. This assumption can help alleviate the possibility of predicting excessive settlement. For permeable natural soil, the vertical hydraulic conductivity  $k_v$  was determined via laboratory permeability test and horizontal hydraulic conductivity  $k_h$  was set as 2.0 times the value of  $k_v$  from previous studies on soft soils (Chai et al. 2013, 2014). Because the compaction was conducted on the soilbag reinforcement before the load test, the tensile force has been generated along the bags, thus the initial axial strain of soilbags was set as 10%. The hydraulic conductivity of the soilbag reinforcement was found much larger than that of the soils contained in the soilbag because of the existence of gaps and contact surfaces between soilbags, as determined in a previous study by Liu et al. (2012), and  $k_h$  was found to be nearly 10 times higher than  $k_v$ . Except for apparent cohesion and hydraulic conductivity, the other parameters of the soilbag-reinforced soils were the same as those of the sandy clay contained in the bags. The initial effective stress of the foundation was determined from the numerical simulation of the self-weight consolidation and excavation. The groundwater level was assumed to be 0.5 m below the excavated surface.

#### 2.4 Comparison of predictions and field measurements

Figs. 6 show a comparison of the test results to the numerical results of the loading-settlement curve for unreinforced foundation and soilbag-reinforced foundations. For the unreinforced foundation, as shown in Fig.6a, the ultimate bearing capacity was less than 100 kPa. A steep reduction in the slope of the loading-settlement curve was observed at the settlement of 2.4% of the footing width, indicating foundation failure. For the soilbag-reinforced foundations, there was no clear failure, even at large settlement, as shown in Fig.6 b-c. The maximum bearing capacity was observed for the foundation reinforced by four layers of soilbags, it was approximately 1.79 times larger than that without soilbag reinforcement. In addition, a reduction in the settlement of the foundation reinforced by the soilbag was also observed. However, from the loading-settlement curves of the soilbag-reinforced foundations obtained from the field load tests, settlement was found smaller than that calculated, especially in the early loading stage, possibly because the increase of the compression modulus of the soilbags was not considered in the numerical simulations. Overall, a good agreement was observed between the field test and the numerical results.

The reduction in footing settlement due to the presence of reinforcement can also be quantified in terms of a parameter called Percentage Reduction in Settlement (PRS). PRS is defined as:

$$PRS = \left( \frac{S_0 - S_r}{S_0} \right) \times 100\% \quad (9)$$

where  $S_0$  is the settlement of the unreinforced foundation corresponding to its ultimate bearing capacity, and  $S_r$  is the settlement of reinforced foundation corresponding to footing pressure equal to the ultimate bearing pressure of the unreinforced foundation. The PRS values observed are 19% and 40%, respectively, for soilbag-reinforced foundations with  $n = 2$  and  $n = 4$ . The maximum PRS (40%) was observed for the soilbag-reinforced foundation with  $n = 4$ , where PRS = 40% indicates a 40% reduction in settlement from the reinforced foundation to the unreinforced clay. Hence, the presence of soilbags in the soft foundation can not only increase the bearing capacity, but also substantially reduce the settlement.

Figs. 7 shows the comparison of the tested and numerical loading-vertical stress curves for points at various depths. There is an excellent agreement between the numerical results and the test measurements at E1, E2, and E4, indicating the effectiveness of the numerical method with ECA to model soilbag-reinforced soils. It was found that agreement of earth pressure at E3 inside soilbag layers in the foundation with four layers of soilbag reinforcement is not as well as that inside the natural soils. This may be induced by the soilbag reinforcement layer under the earth pressure transducer was not compacted thoroughly. Fig. 8 shows the variations of normalized vertical stress with depth for various types of case. These values correspond to the points exactly below the centre of the footing at various depths. The vertical stress  $\sigma_v$  at different depth was normalized by applied pressure  $p$ . Here, the applied pressure was equal to the ultimate bearing capacity of the unreinforced foundation, and the normalized vertical stress measured at locations E1 to E4 were plotted for comparison. A remarkable reduction in the vertical stress of the soilbag reinforcement was found. The maximum stress reduction was observed for the soilbag-reinforced foundation with  $n = 4$ . For the soilbag-reinforced foundations, the calculated stress reduction was a little less than that measured in the field tests, which may be attributed to the increase of the compression modulus of the soilbag not considered in the numerical model.

Figs. 9 shows the numerical results of the vertical stress contour for various test cases. The reported stress contours correspond to the vertical pressure equal to the ultimate bearing capacity of the unreinforced foundation. For the unreinforced foundation, higher stress was observed below the loading plate and transferred to the deeper soils. However, stresses are transferred laterally to the wider areas through the reinforcement for the soilbag-reinforced foundations, reducing the stress in the subgrade. Furthermore, vertical stress was dispersed to the larger areas with increased thickness of soilbag reinforcement. Hegde and Sitharam (2015) observed a similar phenomenon in geocell-reinforced foundation. Matsuoka and Liu (2006) explained the dispersion of vertical stress in foundations reinforced by soilbags, as shown in Fig. 10. The stress dispersion area is directly proportional to the thickness of the soilbag reinforcement embedded in the foundation ( $H_s$ ) and the stress dispersion angle ( $\beta$ ). With the load distributed to the wider area, the overall stress intensity in the subgrade soils decreases. Thereby, the effect of the thickness of soilbag reinforcement is significant, which would improve the overall performance of the reinforced foundation. However, because the thickness of the soilbag reinforcement did not vary significantly in this study, this effect was less obvious.

Fig. 11 presents the distributions of apparent cohesion in the soilbag layers for foundations with two and four layers of soilbag reinforcement when 200 kPa vertical pressure is applied. It can be seen that apparent cohesion of the soilbag layers is largely induced by the dynamic compaction before compression. Thus, the denser the soilbag layer after compaction, the larger the bearing capacity of the soilbag-reinforced foundation. With increase of applied pressure, the compression deformation of the soilbags under the loading plate is larger than at other locations, and so a larger apparent cohesion is generated in this zone. In addition, apparent cohesion is a little larger for the foundation reinforced by two layers of soilbags than by four layers. The compression deformation of the soilbags using four layers of soilbag-reinforced foundation is smaller. Fig. 12 shows the development of apparent cohesion with applied pressure for the soilbag in the second layer under the loading plate. It can be seen that the apparent cohesion increases slowly with the applied pressure at the beginning of the field load test. The compression deformation of the soilbag is small at this stage. With the increase of applied pressure, a turning point appears, and apparent cohesion increases markedly thereafter. The applied pressures corresponding to the turning points are close to the bearing capacities of the soilbag-reinforced foundations with  $n = 2$  and  $n = 4$  layers, which means the larger compression deformation occurred once the applied pressure approaches the bearing capacity. Thus, the results of this analysis confirm the importance of the high-quality compaction of the soilbag reinforcement during construction. This is because of the increase of apparent cohesion with applied pressure is limited before failure of the foundation.

Comparisons of the measured and predicted excess pore water pressure at locations P1 to P3 (see Fig. 2 for the locations) are shown in Fig. 13, respectively. Good excess pore water pressure agreement at locations P1 to P3 can be obtained using the numerical method with ECA. Additionally, the estimated vertical and horizontal hydraulic conductivities of the soilbag reinforcement seemed reasonable. It is worth to point out, the soilbag reinforcement was placed above the groundwater level, the soilbag-reinforced soil was in the condition of unsaturated, and the excess pore water pressure inside soilbag layers has not been measured. Thus, the comparison of excess pore water pressure inside the soilbag reinforcement was not given in this study. Fig. 14 shows the variation of excess pore water pressure with depth for three tests. The values in this figure correspond to the points exactly below the centre of the footing at various depths. Vertical pressure was equal to the ultimate bearing capacity of the unreinforced foundation. A significant reduction in excess pore water pressure was observed at the depth of 0 to 2 m for the soilbag-reinforced foundation. Moreover, the reduction of excess pore water pressure becomes clearer as the thickness of the soilbag reinforcement increases. This is mainly attributed to the dispersion of the ground stress through the soilbag reinforcement, which decreases the additional stress transferred to the deeper foundation and reduces the excess pore water pressure. Besides, for the foundation reinforced with four soilbag layers, it can be found that excess pore water pressure at the depth of 0.1 to 0.4m was more uniform and smaller than that without reinforcement or with two layers of soilbag reinforcement. This can be explained by the high permeability of the soilbag reinforcement,

which reduces the excess pore water pressure in the reinforcement under external load conditions. Thus, with the increasing thickness of soilbag reinforcement, the smaller and more uniform distribution of the excess pore water pressure were generated in the reinforcement. According to this study, it is found that soilbag reinforcement in soft foundations can not only increase bearing capacity, but also reduce the excess pore water pressure generated in the soft foundation under loading condition.

### **3. Conclusions**

This paper presents the results of field load tests and numerical simulations to evaluate the reinforcement effect of soilbags filled with excavated soft soils and the number of soilbag layers, which can be used to improve the bearing capacity of the soft foundation. It was found that soilbag reinforcement with the reused excavated soft soils as the contained material can increase the bearing capacity of soft foundations and reduce settlement under external loads. The bearing capacity and elastic modulus of the reinforced foundation can increase with the greater thickness of the soilbag reinforcement. This was related to the generation of the stress dispersion through the soilbag reinforcement. The larger the thickness of the soilbag reinforcement, the smaller the load transferred to the underlying soft soils. High-quality compaction of the soilbag layers during construction is important to improvement the bearing capacity. In addition, the excess pore water pressure generated in the soft foundation was found to decrease significantly with the help of soilbag reinforcement. Due to the high permeability of the soilbag-reinforced soil, smaller excess pore water pressure and more uniform load distribution was observed in the soilbag reinforcement with the increasing soilbag layer thickness. Comparison of the simulated results to the experimental results of the field load tests showed that the equivalent composite approach (ECA) method introduced in this paper can simulate the deformation of foundations reinforced by soilbags filled with excavated soft soils under vertical loading conditions.

### **Acknowledgements**

The authors wish to express their sincere gratitude to the Fundamental Research Funds for the Central Universities (2019B11214), the Joint Funds of the National Natural Science Foundation of China (U1765205). The first author is grateful for the financial support from the China Scholarship Council (CSC) (201806715020) for his joint research at UPC, Barcelona Tech. We thank the reviewers and the editor for their comments and suggestions to improve the paper.

## Notation

Basic SI units are shown in parentheses.

$B$ : width of soilbag (m)

$B_0$ : initial width of soilbag (m)

$C_c$ : compression index ( $\text{Pa}^{-1}$ )

$c_T$ : apparent cohesion of soilbag (Pa)

$e_0$ : initial void ratio (dimensionless)

$H$ : height of soilbag (m)

$H_0$ : initial height of soilbag (m)

$k$ : tensile stiffness of woven bag (N/m)

$k_h$ : horizontal hydraulic conductivity of foundation soil (m/s)

$k_v$ : vertical hydraulic conductivity of the foundation soil (m/s)

$M$ : slope of the critical state line (dimensionless)

$m$ : initial width to height ratio of soilbag  $B_0/H_0$  (dimensionless)

$n$ : number of soilbag reinforcement layers (dimensionless)

$\hat{p}'$ : translated mean effective stress (Pa)

$p_c$  : pre-consolidation pressure (Pa)

$p_{c0}$ : initial pre-consolidation pressure (Pa)

$q$ : deviatoric stress (Pa)

$S_0$ : settlement of the unreinforced foundation corresponding to its ultimate bearing capacity  
(m)

$S_r$ : settlement of the reinforced foundation corresponding to footing pressure equal to the  
ultimate bearing pressure of the unreinforced foundation (m)

$T$ : bag tensile force (N)

$\delta_{ij}$ : Kronecker's delta (dimensionless)

$\varepsilon_a$ : axial strain in the vertical direction of the soilbags (dimensionless)

$\varepsilon_c$ : circumferential extension strain of the woven bags (dimensionless)

$\varepsilon_v^p$ : plastic volumetric strain (dimensionless)

$\varphi$ : internal friction angle of the material inside the bags ( $^\circ$ )

$\kappa$ : swelling index (dimensionless)

$\lambda$ : compression index (dimensionless)

$\sigma_0$ : bonding stress induced by cohesion (Pa)

$\sigma_1$  : vertical major principal stress of the soilbags (Pa)

$\sigma_3$  : horizontal minor principal stress of the soilbags (Pa)

$\sigma_{01}$  : additional major principal stress produced by the tension of the bag (Pa)

$\sigma_{03}$  : additional minor principal stress produced by the tension of the bag (Pa)

$\sigma_{ij}$  : stress tensor (Pa)

### **Abbreviations**

ECA    equivalent composite approach

## References

- Ansari, Y., Merifield, R., Yamamoto, H., Sheng, D. (2011). Numerical analysis of soilbags under compression and cyclic shear. *Computers and Geotechnics*, **38**, No. 5, 659-668.
- Basudhar, P. K., Dixit, P. M., Gharpure, A., Deb, K. (2008). Finite element analysis of geotextile-reinforced sand-bed subjected to strip loading. *Geotextiles and Geomembranes*, **26**, No. 1, 91-99.
- Bathurst, R. J., Karpurapu, R., (1993). Large-scale triaxial compression testing of geocellreinforced granular soils. *Geotech. Test J.* **16**, No. 3, 296–303.
- Bathurst, R. J., Knight, M. A. (1998). Analysis of geocell reinforced-soil covers over large span conduits. *Computers and Geotechnics*, **22**, No. 3, 205-219.
- Bergado, D. T., Teerawattanasuk, C. (2008). 2D and 3D numerical simulations of reinforced embankments on soft ground. *Geotextiles and Geomembranes*, **26**, No. 1, 39-55.
- Chai, J., Igaya, Y., Hino, T., Carter, J. (2013). Finite element simulation of an embankment on soft clay - Case study. *Computers and Geotechnics*, **48**, No. 1, 117-126.
- Chai, J., Shen, S., Ding, W., Zhu, H., Carter, J. (2014). Numerical investigation of the failure of a building in Shanghai, China. *Computers and Geotechnics*, **55**, No. 1, 482-493.
- Chen, R. H., Huang, Y. W., Huang, F. C. (2013a). Confinement effect of geocells on sand samples under triaxial compression. *Geotextiles and Geomembranes*, **39**, No. 8, 51-62.
- Chen, R. H., Wu, C. P., Huang, F. C., Shen, C.W. (2013b). Numerical analysis of geocell-reinforced retaining structures. *Geotextiles and Geomembranes*, **37**, No. 3, 35-44.
- Cheng, H. & Yamamoto, H. (2016a). Modeling microscopic behavior of geotextile-wrapped soil by discrete element method. *Japanese Geotechnical Society Special Publication*, **2**, No. 65, 2215–2220.
- Cheng, H., Yamamoto, H. & Thoeni, K. (2016b). Numerical study on stress states and fabric anisotropies in soilbags using the DEM. *Computers and Geotechnics*, **76**, 170–183.
- Hataf, N., & Sayadi, M. (2018). Experimental and numerical study on the bearing capacity of soils reinforced using geobags. *Journal of Building Engineering*, **15**, 290-297.
- Hegde, A., Sitharam, T. G. (2013). Experimental and numerical studies on footings supported on geocell reinforced sand and clay beds. *International Journal of Geotechnical Engineering*, **7**, No. 4, 347-354.
- Hegde, A., Sitharam, T. G. (2015). 3-Dimensional numerical modelling of geocell reinforced sand beds. *Geotextiles and Geomembranes*, **43**, No. 2, 171-181.
- Hornsey, W. P., Carley, J. T., Coghlan, I. R., Cox, R. J. (2011). Geotextile sand container shoreline protection systems: Design and application. *Geotextiles and Geomembranes*, **29**, No. 4, 425-439.
- Indraratna, B., Asce, F., Biabani, M. M., Nimbalkar, S. (2014). Behavior of Geocell-Reinforced Subballast Subjected to Cyclic Loading in Plane-Strain Condition. *Journal of Geotechnical & Geoenvironmental Engineering*, **141**, No. 1, 04014081.
- Indraratna, B., Nimbalkar, S., Christie, D., Rujikiatkamjorn, C., Vinod, J. (2010). Field Assessment of the Performance of a Ballasted Rail Track with and without

- Geosynthetics. *Journal of Geotechnical & Geoenvironmental Engineering*, **136**, No. 7, 907-917.
- Kim, H. J., Won, M. S., Lee, K. H., Jamin, J. C. (2015). Model Tests on Dredged Soil-Filled Geocontainers Used as Containment Dikes for the Saemangeum Reclamation Project in South Korea. *International Journal of Geomechanics*, **16**, No. 2, 04015055.
- Kim, M., Freeman, M., FitzPatrick, B. T., Nevius, D. B., Plaut, R. H., Filz, G. M. (2004). Use of an apron to stabilize geomembrane tubes for fighting floods. *Geotextiles and Geomembranes*, **22**, No. 4, 239-254.
- Lee, S. M., Choi, C., Shin, E. C. (2013). A study of connection stability for reinforced retaining wall constructed with soilbag with varying connection strength. *J. Korean Geosynth. Soc.* **12**, No. 1, 101-107. (in Korean)
- Leshchinsky, B., Ling, H. I. (2013). Numerical modeling of behavior of railway ballasted structure with geocell confinement. *Geotextiles and Geomembranes*, **36**, No. 1, 33-43.
- Li, Z., Liu, S. H., Wang, L. J., Zhang, C. C. (2013). Experimental study on the effect of frost heave prevention using soilbags. *Cold Regions Science and Technology*, **85**, No. 1, 109-116.
- Liu, S. H., Bai, F. Q., Wang, Y. S., Wang, S., Li, Z. (2012). Treatment for expansive soil channel slope with soilbags. *J. Aerosp. Eng.* **26**, 657-666.
- Liu, S. H., Fan, K. W., Xu, S. Y. (2019). Field study of a retaining wall constructed with clay-filled soilbags. *Geotextiles and Geomembranes*, **49**, No. 1, 87-94.
- Liu, S. H., Gao, J. J., Wang, Y. Q., Weng, L. P. (2014). Experimental study on vibration reduction by using soilbags. *Geotextiles and Geomembranes*, **42**, No. 1, 52-62.
- Liu, S. H., Jia, F., Shen, C. M., Weng, L. P. (2018). Strength characteristics of soilbags under inclined loads. *Geotextiles and Geomembranes*, **46**, No. 1, 1-10.
- Liu, S. H., Lu, Y., Weng, L. P., Bai, F. Q. (2015). Field study of treatment for expansive soil/rock channel slope with soilbags. *Geotextiles and Geomembranes*, **43**, No. 4, 283-292.
- Liu, S. H., Matsuoka, H. (2007). A new earth reinforcement method by soilbags. *Rock and Soil Mechanics*, **28**, No. 8, 1665-1670. (in Chinese)
- Liu, S. H., Wang, L. J., Wang, Z. J., Bauer, E. (2016). Numerical stress-deformation analysis of cut-off wall in clay-core rockfill dam on thick overburden. *Water Science and Engineering*, **9**, No. 3, 219-226.
- Martinelli, L., Zanuttigh, B., De Nigris, N., Preti, M. (2011). Sandbag barriers for coastal protection along the Emilia Romagna littoral, Northern Adriatic Sea, Italy. *Geotextiles and Geomembranes*, **29**, No. 4, 370-380.
- Matsuoka, H. (2000a). Construction cases of retaining walls and building foundation improvement by soilbags, in: *Proc. of the 35th Japan National Conf. on Geotech. Engrg.* pp. 1077-1078. (in Japanese)
- Matsuoka, H., Chen, Y., Kodama, H., Yamaji, Y., Tanaka, R. (2000b). Mechanical properties of soilbags and unconfined compression tests on model and real soilbags, in: *Proc. of the 35th Japan National Conf. on Geotech. Engrg.* 544, 1075-1076. (in Japanese)

- Matsuoka, H. & Liu, S.H. (1999). Bearing capacity improvement by wrapping a part of foundation. *Japan Society of Civil Engineers (JSCE)*, No.617/III-46, 235–249 (in Japanese).
- Matsuoka, H., Liu, S. H. (2003). New earth reinforcement method by soilbags (“Donow”). *Soils and Foundations*, **43**, 173–188.
- Matsuoka, H., Liu, S.H. (2006). *A new earth reinforcement method using soil bags*, Taylor & Francis/Balkema, The Netherlands.
- Matsuoka, H., and Sun, D. A. (1995). Extension of spatially mobilized plane (SMP) to frictional and cohesive materials and its application to cemented sands. *Soils and Foundations*, **35**, No. 4, 63–72.
- Matsuoka, H., Sun, D. A., Kogane, A., Fukuzawa, N., Ichihara, W. (2002). Stress–strain behaviour of unsaturated soil in true triaxial tests. *Can. Geotech. J.* **39**, 608–619.
- Mehdipour, I., Ghazavi, M., Moayed, R. Z. (2013). Numerical study on stability analysis of geocell reinforced slopes by considering the bending effect. *Geotextiles and Geomembranes*, **37**, No. 37, 23–34.
- Miyata, Y., Bathurst, R.J. and Miyatake, H. (2015). Performance of three geogrid-reinforced soil walls before and after foundation failure. *Geosynthetics International*, **22**, No. 4, 311–326.
- Moreira, A., Vieira, C. S., das Neves, L., Lopes, M. L. (2016). Assessment of friction properties at geotextile encapsulated-sand systems’ interfaces used for coastal protection. *Geotextiles and Geomembranes*, **44**, No. 3, 278-286.
- Muramatsu, D., Ye, B. & Zhang, F. (2009). Numerical Simulation of Vibration Damping Effect of Soilbag. *Japanese Geotechnical Journal*, **4**, No. 1, 71–80. (in Japanese)
- Muramatsu, D., Zhang, F., Shahin, H. M. (2007). Numerical simulation on bearing capacity of soilbag-reinforced ground considering finite deformation. *Japanese Geotechnical Journal*, **2**, No. 1, 11–23.
- Rahimi, M., Leshchinsky, B. and Moghaddas Tafreshi, S. N. (2018a). Assessing the ultimate uplift capacity of plate anchors in geocell-reinforced sand. *Geosynthetics International*, **25**, No. 6, 612-629.
- Rahimi, M., Moghaddas Tafreshi, S.N., Leshchinsky, B., and Dawson, A. R. (2018b). Experimental and numerical investigation of the uplift capacity of plate anchors in geocell-reinforced sand, *Geotextiles and Geomembranes*, **46**, No. 6, 801-816.
- Rajagopal, K., Krishnaswamy, N. R., Madhavi Latha, G. (1999). Behavior of sand confined with single and multiple geocells. *Geotextiles and Geomembranes*, **17**, No. 3, 171–184.
- Rowe, R.K., Taechakumthorn, C. (2008). Combined effect of PVDs and reinforcement on embankments over rate-sensitive soils. *Geotextiles and Geomembranes*, **26**, No. 3, 239-249.
- Rowe, R.K., Taechakumthorn, C. (2011). Design of reinforced embankments on soft clay deposits considering the viscosity of both foundation and reinforcement. *Geotextiles and Geomembranes*, **29**, No. 5, 448-461.

- Shao, J. X., Huang, J., Zhou, B. M. (2005). Application of soil bags in subgrade engineering. *Highway*, **7**, 82–86. (in Chinese)
- Song, F., Liu, H., Ma, L., Hu, H. (2018). Numerical analysis of geocell-reinforced retaining wall failure modes. *Geotextiles and Geomembranes*, **46**, No. 3, 284-296.
- Song, F., Liu, H. B., Chai, H. B., Chen, J. X. (2017). Stability analysis of geocell-reinforced retaining walls. *Geosynthetics International*. **24**, No. 5, 442–450.
- Tantono, S. F., Bauer, E. (2008). Numerical simulation of a soil bag under vertical compression, in: *The 12th International Conference of International Association for Computer Methods and Advances in Geomechanics (IACMAG)*, Goa, India. pp. 1–5.
- Wang, L. J., Liu, S. H., Fu, Z. Z., Li, Z. (2015). Coupled hydro-mechanical analysis of slope under rainfall using modified elasto-plastic model for unsaturated soils. *J. Cent. South Univ.*, **22**, 1892-1900.
- Wang, L. J., Liu, S. H., Zhou, B. (2015). Experimental study on the inclusion of soilbags in retaining walls constructed in expansive soils. *Geotextiles and Geomembranes*, **43**, No. 1, 89–96.
- Wen, H., Wu, J., Zou, J., Luo, X., Zhang, M., Gu, C. (2016). Model tests on the retaining walls constructed from geobags filled with construction waste. *Adv. Mater. Sci. Eng.* **21**, No. 6, 2317–2330.
- Xu, Y., Huang, J., Du, Y., Sun, D. (2008). Earth reinforcement using soilbags. *Geotextiles and Geomembranes*, **26**, No. 3, 279–289.
- Xu, Y.F., Zhou, B.M., Tong, L.X. (2007). Tests on soilbags. *J. Highway Transport. Res. Dev.* **9**, 84–88 (in Chinese).
- Ye, B., Muramatsu, D, Ye, G. L., Zhang F. (2011). Numerical assessment of vibration damping effect of soilbags. *Geosynthetics International*, **18**, No. 4, 159–168.

**Table Captions**

Table 1. Geotechnical properties of foundation soils.

Table 2. Results of field load tests.

Table 3 Model parameters for numerical simulations.

Table 1. Geotechnical properties of foundation soils

Geotechnical property	Silty clay	Infilled sandy clay
Initial water content, $w_0$ (%)	46.5	20.1
Liquid limit, $w_L$ (%)	43.9	29.1
Plastic limit, $w_p$ (%)	24.2	18.2
Plasticity index, $I_p$ (%)	19.7	10.9
Initial void ratio, $e_0$	1.4	0.6
Specific gravity, $G_s$	2.74	2.67
Compression index, $C_c$	1.5	0.12
Hydraulic conductivity, $k_v$ ( $10^{-8}$ m/s)	5	40
Pre-consolidation pressure, $p_{c0}$ (kPa)	100	80

Table 2 Results of field load tests

Types of foundation	Ultimate bearing capacity $q_{cr}$ (kPa)	Ultimate settlement $s_{cr}$ (mm)	Elastic modulus $E_0$ (MPa)
Unreinforced foundation	96	24.1	3.55
Soilbag-reinforced foundation with $n = 2$	135	26.4	4.92
Soilbag-reinforced foundation with $n = 4$	170	31.8	6.26

Table 3 Model parameters for numerical simulations

Soil type	M	$\lambda$	$\kappa$	$\mu$	$e_0$	c (kPa)	$\gamma_t$ ( $\text{kN/m}^3$ )	$k_v$ ( $10^{-8}$ m/s)	$k_h$
Silty clay	1.0	0.65	0.065	0.3	1.4	20	16.8	5	10
Infilled sandy clay	1.2	0.02	0.002	0.3	0.6	203	18.1	500	5000

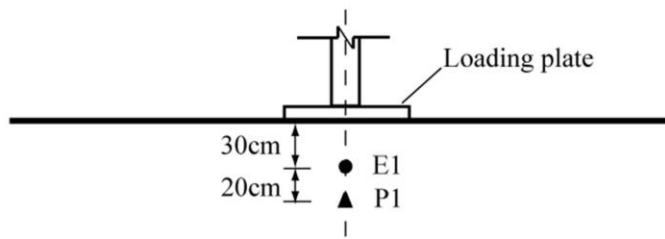
**Figure Captions**

- Fig. 1. Plate load tests for (a) undisturbed soil foundations and (b) foundations reinforced by soil bags.
- Fig. 2. Transducer sketch map.
- Fig. 3. Installation of transducers in natural soil during the (a) excavation step and (b) backfilling step.
- Fig. 4. Stresses acting on two-dimensional model soilbag and on particles inside the soilbag: (a) Stresses acting on soilbag; (b) Stresses acting on particles inside soilbag.
- Fig. 5. Mesh and boundary conditions.
- Fig. 6. Comparison of loading-settlement curves for different types of foundation.
- Fig. 7. Comparison of loading-vertical stress curves.
- Fig. 8. Variation of normalized vertical stress with depth.
- Fig. 9. Contours of vertical stress: (a) unreinforced; (b) reinforcement with two layers of soil bags; (c) reinforcement with four layers of soil bags.
- Fig. 10. Schematic view of vertical stress dispersion under reinforcement with soil bags.
- Fig. 11. Contours of apparent cohesion in the soilbag layers with applied pressure 200kPa.
- Fig. 12. Development of apparent cohesion with applied pressure for soilbag under loading plate in the second layer.
- Fig. 13. Comparison of excess pore water pressure-loading curves.
- Fig. 14. Variation of excess pore water pressure with depth for various cases.

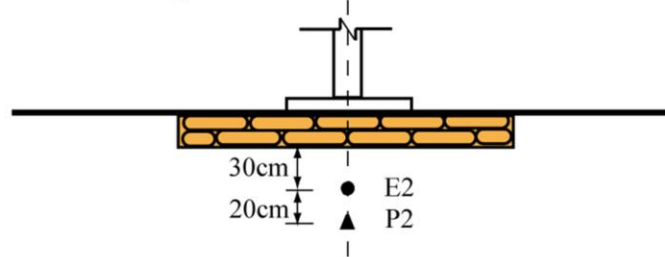


Fig. 1

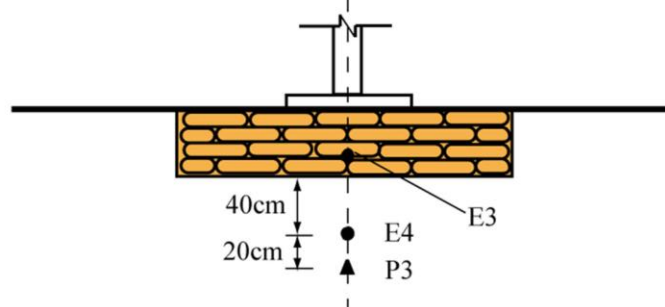
Case A. Unreinforced foundation



Case B. Soilbag-reinforced foundation with n=2



Case C. Soilbag-reinforced foundation with n=4



E1-E4: Earth pressure transducer

P1-P3: Pore water pressure transducer

Fig. 2

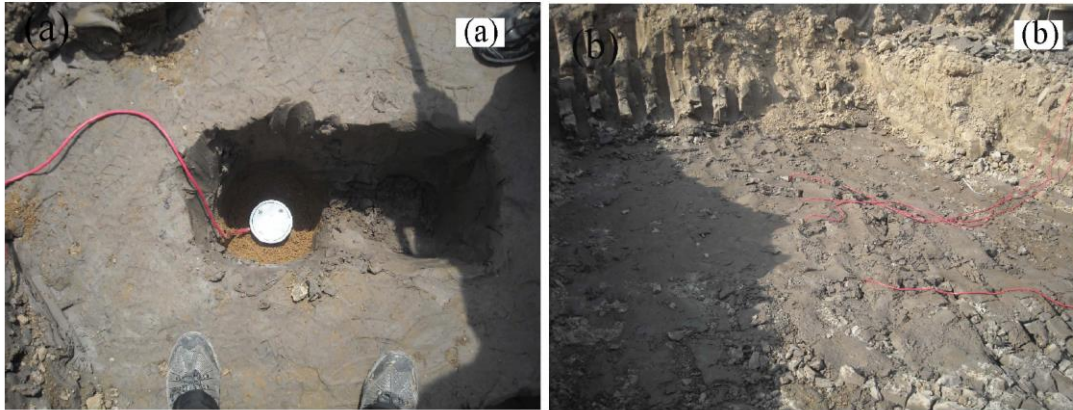
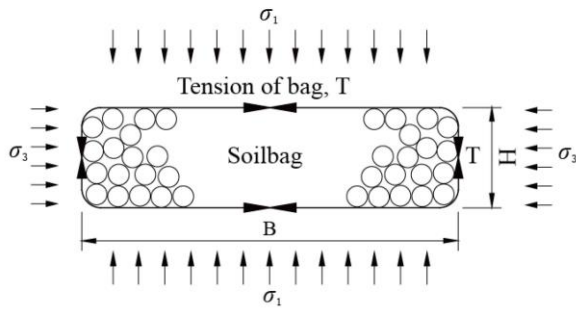
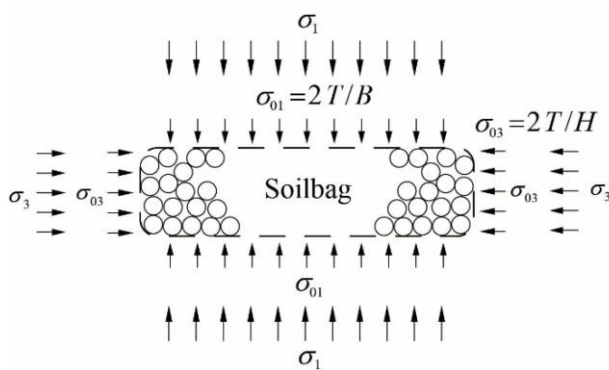


Fig. 3



(a) Stresses acting on soilbag



(b) Stresses acting on particles inside soilbag

Fig. 4

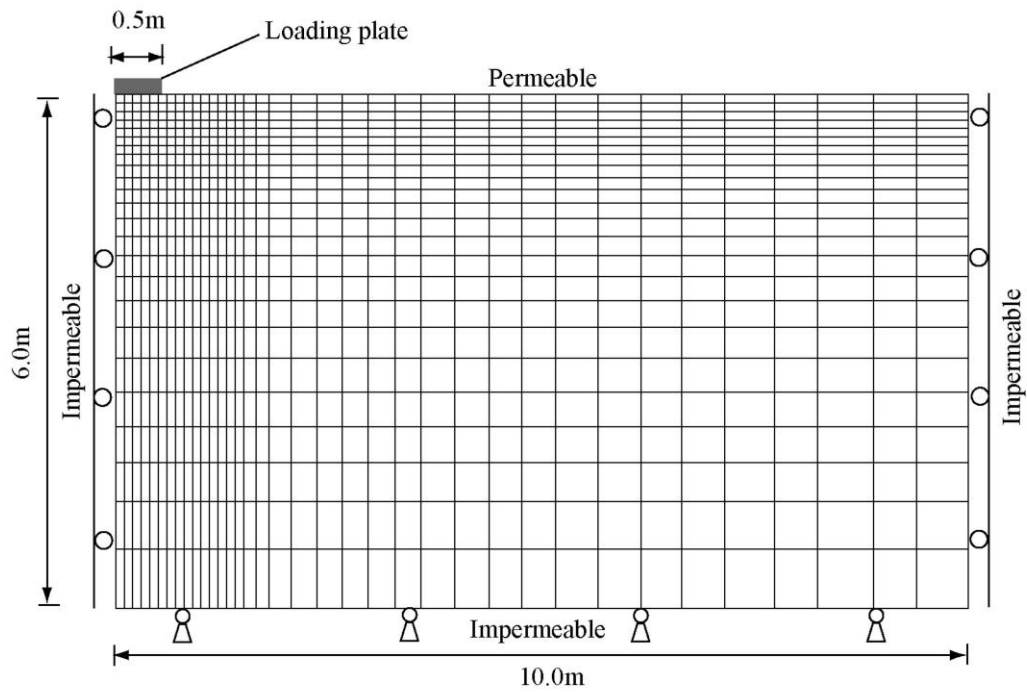
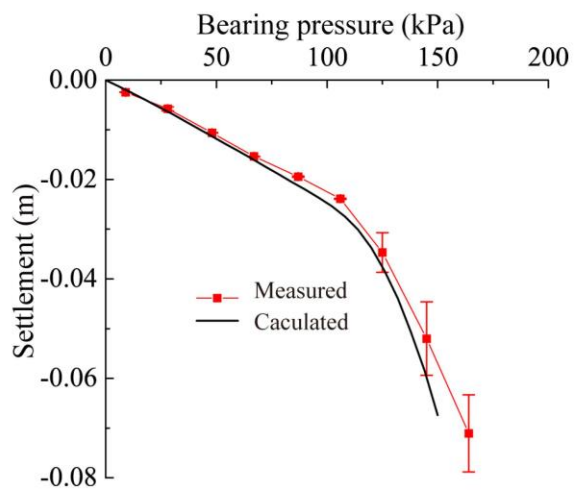
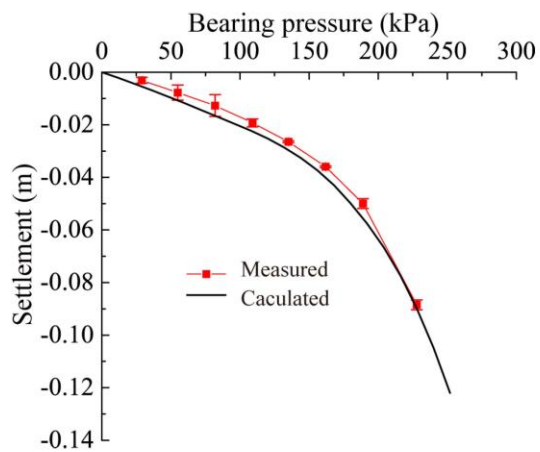


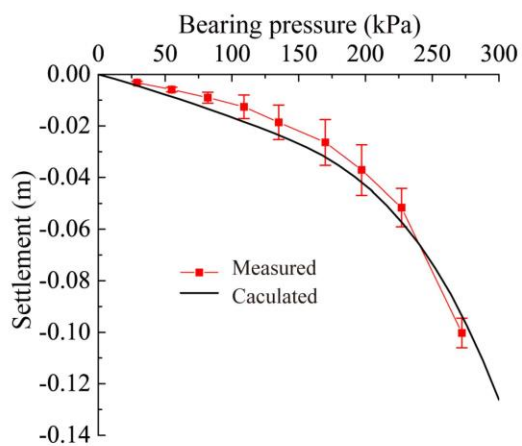
Fig. 5



(a) Unreinforced foundation



(b) Soilbag-reinforced foundation with  $n = 2$



(c) Soilbag-reinforced foundation with  $n = 4$

Fig. 6

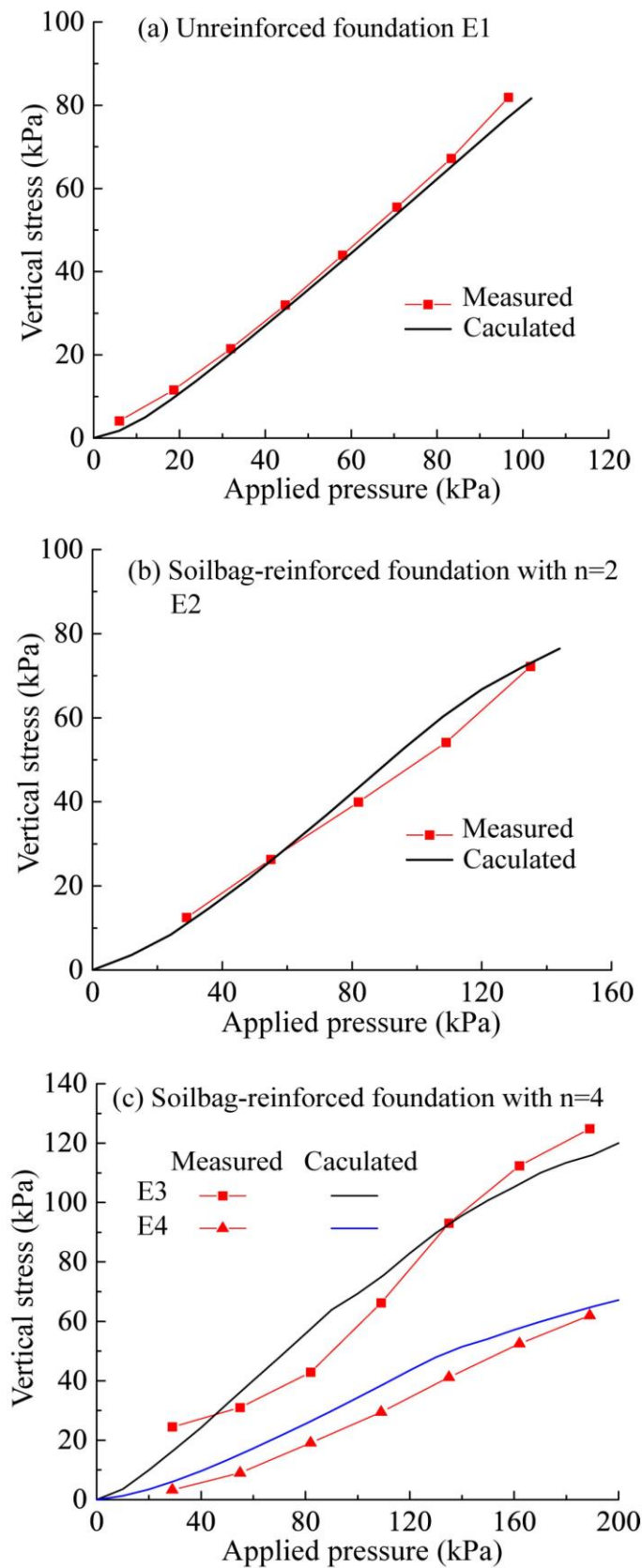


Fig. 7

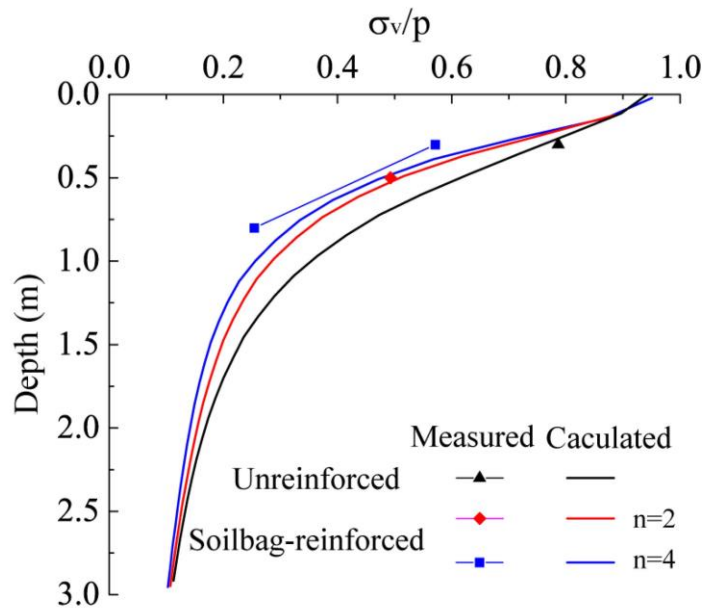


Fig. 8

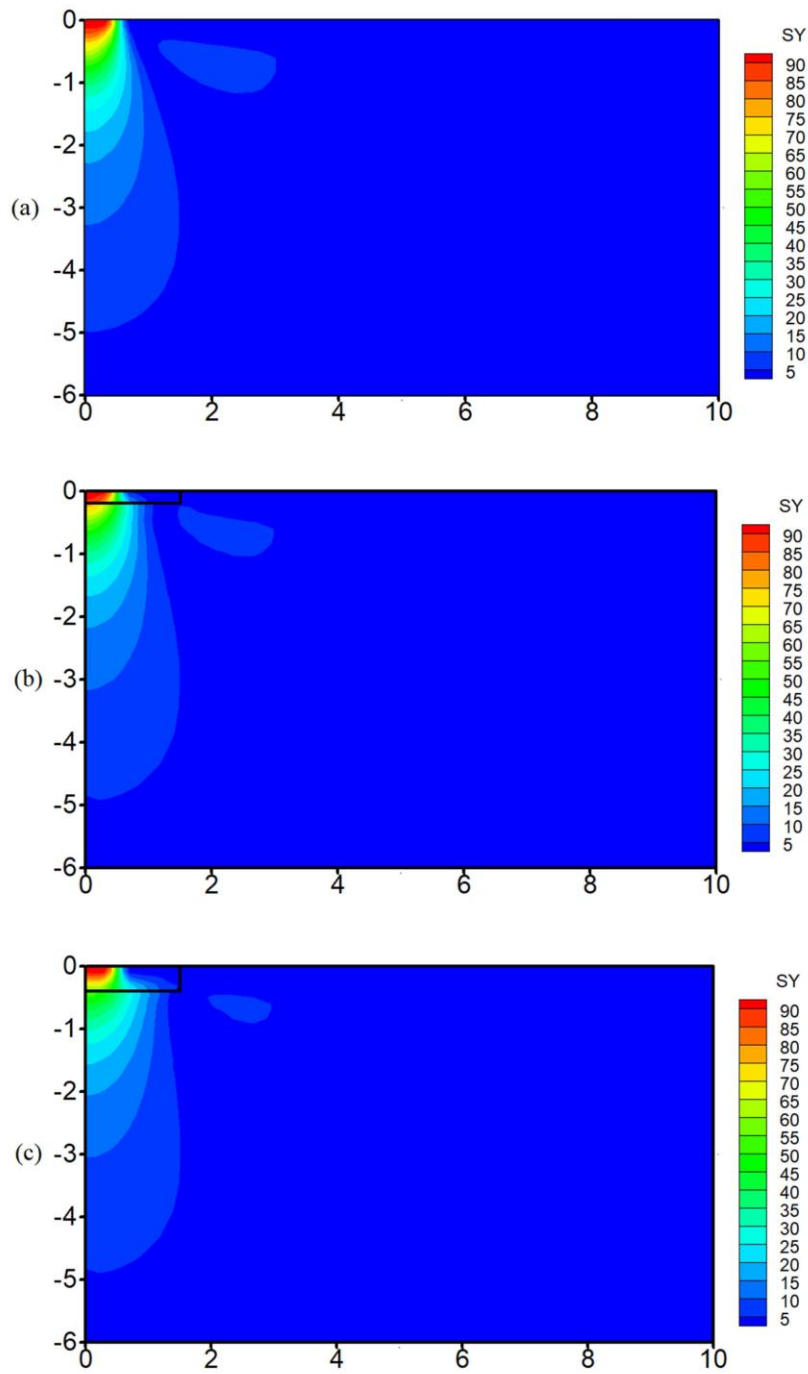


Fig. 9

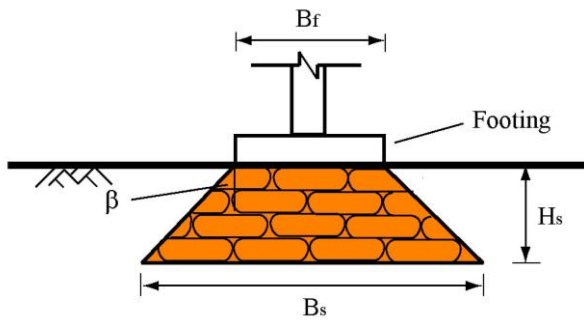


Fig. 10

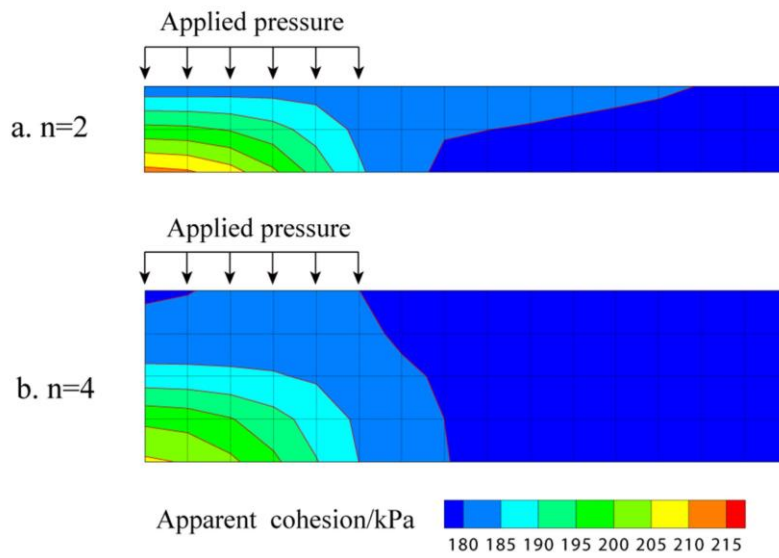


Fig. 11

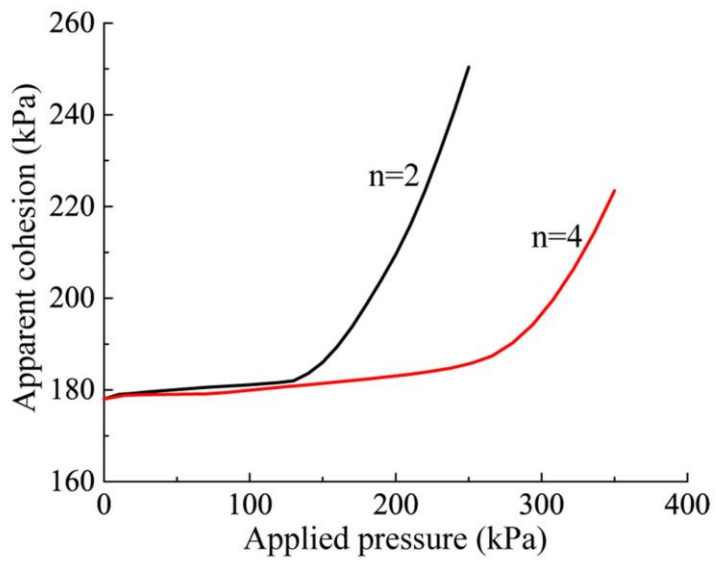


Fig. 12

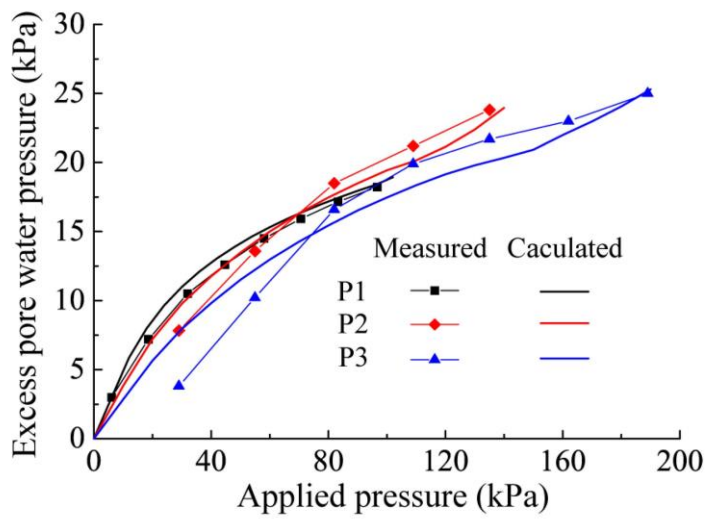


Fig. 13

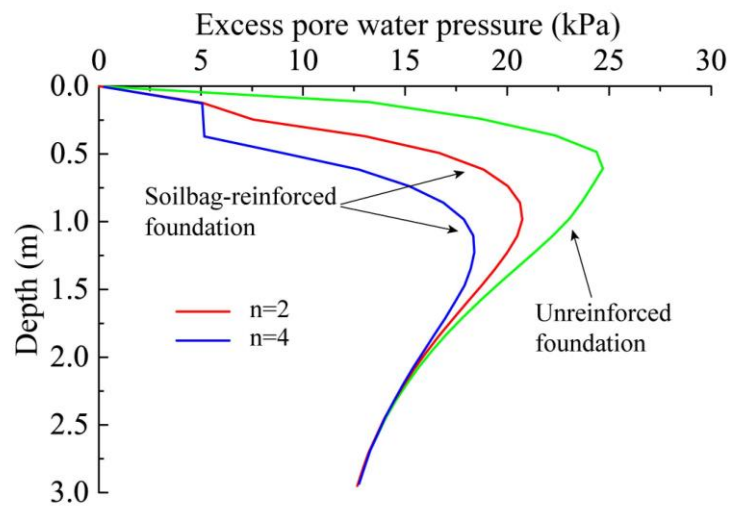


Fig. 14